Mechanosensitivity of astrocytes on optimized polyacrylamide gels analyzed by quantitative morphometry

2010 J. Phys.: Condens. Matter 22 194114

(http://iopscience.iop.org/0953-8984/22/19/194114)

J. Phys.: Condens. Matter **22** (2010) 194114 (11pp) doi:10.1088/0953-8984/22/19/194114

Mechanosensitivity of astrocytes on optimized polyacrylamide gels analyzed by quantitative morphometry

Pouria Moshayedi[1,2], Luciano da F Costa[3,4], Andreas Christ[1], Stephanie P Lacour[5], James Fawcett[2], Jochen Guck[1,7] and Kristian Franze[1,6]

[1] Department of Physics, Cavendish Laboratory, University of Cambridge, J J Thomson Avenue, Cambridge CB3 0HE, UK
[2] Cambridge Centre for Brain Repair, University of Cambridge, ED Adrian Building, Forvie Site, Robinson Way, Cambridge CB2 0PY, UK
[3] Instituto de Física de São Carlos, University of São Paulo, São Carlos, Brazil
[4] National Institute of Science and Technology for Complex Systems, Brazil
[5] Nanoscience Centre, University of Cambridge, 11 J J Thomson Avenue, Cambridge CB3 0FF, UK
[6] Department of Physiology, Development and Neuroscience, University of Cambridge, Downing Street, Cambridge CB2 3DY, UK

E-mail: jg473@cam.ac.uk

Received 16 October 2009, in final form 10 February 2010
Published 26 April 2010
Online at stacks.iop.org/JPhysCM/22/194114

Abstract

Cells are able to detect and respond to mechanical cues from their environment. Previous studies have investigated this mechanosensitivity on various cell types, including neural cells such as astrocytes. In this study, we have carefully optimized polyacrylamide gels, commonly used as compliant growth substrates, considering their homogeneity in surface topography, mechanical properties, and coating density, and identified several potential pitfalls for the purpose of mechanosensitivity studies. The resulting astrocyte response to growth on substrates with shear storage moduli of $G' = 100$ Pa and $G' = 10$ kPa was then evaluated as a function of coating density of poly-D-lysine using quantitative morphometric analysis. Astrocytes cultured on stiff substrates showed significantly increased perimeter, area, diameter, elongation, number of extremities and overall complexity if compared to those cultured on compliant substrates. A statistically significant difference in the overall morphological score was confirmed with an artificial intelligence-based shape analysis. The dependence of the cells' morphology on PDL coating density seemed to be weak compared to the effect of the substrate stiffness and was slightly biphasic, with a maximum at 10–100 μg ml^{-1} PDL concentration. Our finding suggests that the compliance of the surrounding tissue *in vivo* may influence astrocyte morphology and behavior.

(Some figures in this article are in colour only in the electronic version)

1. Introduction

Cells in tissues are mainly surrounded by other cells and extracellular matrix (ECM). They establish contacts with adjacent cells and ECM structures through different surface protein receptors as anchorage points. Cells as the dynamic building blocks of the body receive various cues from their environment and respond accordingly by adopting their metabolism and shape. Until recently, these cues were considered to be solely 'biological' and relayed through ligand–receptor interactions. However, many cell receptors are integrated with the force-generating machinery of the

[7] Author to whom any correspondence should be addressed.

cytoskeleton through focal adhesion proteins, so that internal biochemical responses can also be triggered by external or internal force-generating mechanisms [1–4]. In other words, cells may operate a mechano-sensory system that feels the surrounding environment. Thus, mechanical properties of the cells' environment are part of the information that cells may receive and respond to [5–7].

In various cell types, many cell properties are influenced by the mechanical properties of the substrate on which they grow, including cell attachment [8, 9], shape [8, 10–12], proliferation [13, 14], motility [12, 15–19], and differentiation [1, 14, 20–23]. Consequently, *in vivo*, the compliance of tissues is in a range where cells perform their 'normal' functions. In some diseases, however, a change in stiffness of the affected tissues is partly accountable for the cells' loss of their physiological functions [24–27]. Mechanical properties of cells, tissues, and implants have increasingly been considered in tissue engineering approaches; the compliance of implanted devices has even been tailored to promote reparative functions in the host tissue [28]. This has also encouraged *in vitro* studies aimed at interrogating cell behavior in response to varying the compliance of growth substrates.

In order to study the effects of substrate stiffness on cell behavior, model microenvironments are required. Hydrogels have been widely applied as a model for ECM. Protein-based gels, including collagen [29], matrigel [30], and fibrin [31], can be tuned over a range of compliances by changing the filamentous protein concentration or by adding biological and chemical factors such as crosslinkers [32]. Alginate and agarose, crosslinked polysaccharides, have also been used to study cell growth on substrates with varying stiffness [33–36]. However, in order to unambiguously identify the influence of mechanical cues on cell behavior it is crucial to vary the substrate stiffness independently of changes in its biological properties. This is difficult, in general, when using biopolymers, as cells can recognize many of them by specific receptor binding, which may then trigger an additional response. Furthermore, in biopolymer gels the mechanical properties are often exclusively controlled by the polymer concentration, which also significantly changes the gels' mesh size, which in turn could provide important topological cues [37].

In light of this problem, studies have resorted to artificial gels. Polyacrylamide (PAA) gels constitute a common example. They are made from acrylamide (AA) polymers crosslinked by bis-acrylamide (Bis-A). By varying the amount of the two components one can obtain a range of elasticities (e.g., characterized by the complex shear modulus $G^*(\omega) = G'(\omega) + \mathrm{i}G''(\omega)$, where the storage modulus G' quantifies a material's elastic response to deformation and the loss modulus G'' contains information about its viscous properties at an angular frequency ω) from $G' \sim 0.01$ to 230 kPa [38, 39]. The PAA gels' stiffness can be varied with negligible effect on the mesh size and no change in biological stimulus to the cells, because they are biologically inert and 'anti-adhesive' materials [32]. Consequently, gels have to be activated and covalently grafted with peptides or proteins in order to prepare them for cell culture. This opens the possibility to independently control the biological properties of the PAA gel surface [32]. Finally, PAA is an isotropic and almost perfectly elastic material (it returns to its original shape once forces are released), which makes traction force calculations by analysis of deformation fields feasible [5, 40, 41]. Due to these advantages, PAA gels have been widely used in cell substrate studies [10–12, 14–16, 19, 20, 23, 24, 34, 39, 42].

Conclusive cell substrate studies necessitate well-characterized surfaces, so that the changes in cell behavior can solely be attributed to substrate stiffness rather than to surface topological cues or inhomogeneities in surface coating [24, 28]. In this study, we identified useful combinations of AA and Bis-A by carefully considering all relevant surface properties. Rheological bulk measurements of PAA gels with elasticities (G') from 0.1 to 30 kPa were quantitatively confirmed on a microscopic scale by scanning force microscopy (SFM). SFM furthermore confirmed the gels to be homogeneous and to possess a smooth surface. In addition, the homogeneity and amount of the surface polypeptide coating was tested using both epifluorescence and confocal laser scanning microscopy. This detailed gel surface analysis revealed several potential pitfalls for the purpose of mechanosensitivity studies, such as mechanical instabilities (crease formation) on the surface of gels made from inappropriate AA:Bis-A ratios.

Astrocytes, glial cells in the central nervous system, were then cultured on these well-defined substrates. Previous studies suggested that the number of astrocytes increased with increasing substrate stiffness [34, 39, 42] or remained constant [43]. Furthermore, it had been qualitatively shown that the cells' phenotype and cytoskeletal content change on different substrates [39, 42, 43]. Here, we quantified the effects of substrate stiffness and polypeptide coating concentration on astrocyte morphological key parameters with automated morphometry techniques.

2. Materials and methods

2.1. Polyacrylamide (PAA) gel fabrication

PAA gels were fabricated on a glass coverslip as described previously [15]. Briefly, 22 mm round glass coverslips (referred to as 'bottom coverslips') were washed with 600 μl of 0.1 N NaOH solution and dried. The coverslips were then treated with 200 μl (3-aminopropyl)trimethoxysilane (APTMS; unless otherwise stated all chemicals from Sigma, UK) and washed thoroughly with distilled water after 3 min. 400 μl of 0.5% glutaraldehyde solution were added to the bottom coverslips, which were washed and air-dried after 30 min. Round glass coverslips of 19 mm diameter ('top coverslips') were washed and submerged in Rain-X solution (Shell Car Care International Ltd, UK) for 10 min and air-dried afterward.

In order to establish a range of PAA gel elasticities, PAA premixes were prepared from volumes of phosphate buffered saline (PBS, Bioclear, UK), 40% AA solution (w/v; Electran BDH, UK) in PBS, and 2% bis-A solution (Fisher Scientific, UK) according to table 1. The solution was desiccated for

Table 1. PAA gels used in this study. The table shows acrylamide (AA, 40%) and bis-acrylamide (Bis-A, 2%) volume percentages and the according storage moduli $G'(\omega)$ acquired at $\omega = 1$ rad s^{-1}.

No	G' (Pa)	AA (%)	Bis-A (%)
1	117 ± 13	5	0.04
2	308 ± 27	5	0.07
3	$1\,227 \pm 70$	7.5	0.06
4	$3\,190 \pm 140$	7.5	0.2
5	$10\,107 \pm 1041$	12	0.2
6	$30\,833 \pm 817$	18	0.4

20 min. To initiate gelation, 1% (v/v) ammonium persulfate and 0.3% (v/v) tetramethylethylenediamine (TEMED; Argos Organics, USA) were mixed with the PAA premixes. Subsequently, 60 μl of the solution were put on a bottom coverslip and gently covered with a top coverslip. After 15 min, gel and coverslips were soaked in PBS for 20 min to facilitate the removal of the top coverslip. The exposed gel was washed in PBS three times for 10, 20, and 30 min. For functionalization, gels were treated with hydrazine hydrate overnight (∼12 h) [44]. The gels were then treated with 5% acetic acid solution (Fisher Scientific, UK) for 1 h and subsequently washed in sterile PBS three times for 10, 20, and 30 min. Finally, the gels were treated with poly-D-lysine solution (PDL, 150–300 kDa; PDL tagged with Alexa-488 for coating measurements, see below) for 1 h at 37 °C and then washed three times with PBS for 10, 20, and 30 min.

2.2. Bulk rheology measurements

Mechanical bulk properties of the gels were measured using a Physica MCR rheometer (Anton Paar, Austria). Measurements were done with a parallel plate (⌀ 50 mm) at 20 °C. Control measurements of gels at 37 °C yielded identical shear moduli (data not shown). The linear elastic region of the gels was assessed at an angular frequency of 10 rad s^{-1} (data not shown), and the frequency-dependent complex shear modulus was determined using an oscillatory shear strain with an amplitude of 2%. The periphery of the gels was soaked in PBS during the experiment to avoid drying.

2.3. Scanning force microscopy

A scanning force microscope (NanoWizard II, JPK Instruments, Germany) mounted on an inverted microscope (Eclipse TE2000-U, Nikon, Japan) was used to measure the local mechanical properties of the PAA gels. Silicon cantilevers (BS-Cont-10, JPK, Germany; nominal spring constants ∼0.2 N m^{-1}) were modified by attaching polystyrene spheres ($R \sim 2.73$ μm, Microparticles GmbH, Germany) to their tip [45, 46]. The cantilever spring constants were measured using a thermal noise calibration method [47]. Gels were mounted in a fluid cell (Biocell, JPK, Germany) at room temperature. Each sample was indented at nine equally spaced points within an area of 100 μm × 100 μm with an approach speed of 1.5 μm s^{-1} [46]. Data was fitted to the Hertz model in order to extract the material's Young's modulus E as described previously [48]: $F = \frac{4}{3}\frac{E}{1-\nu^2}\sqrt{R}\delta^{3/2}$, where F is the force applied, R is the radius of the bead, and δ is the magnitude of indentation. Poisson's ratio ν of the PAA gels was assumed to be 0.48 [49]. SFM was also used in contact mode to scan the surface of random areas of the PAA gels in order to investigate the gels' surface topography.

2.4. Coating measurements

Gels were treated with PDL tagged with a fluorophore (Alexa Fluor-488) and examined by fluorescence microscopy [42]. To conjugate PDL to Alexa Fluor-488, 5 mg PDL were dissolved in 0.5 ml 0.1 M sodium bicarbonate buffer (pH 8.3). Alexa Fluor-488 succinimidyl ester (Molecular Probes, USA) was dissolved in dimethyl sulfoxide (10 mg ml^{-1}) immediately before use. While vortexing the PDL solution, the reactive dye solution was added slowly. The reaction was incubated for 1 h at room temperature with continuous vortexing. Subsequently, the solution was membrane-dialyzed with a 12–14 kDa cut-off threshold against deionized water at 4 °C overnight (D-Tube™ Dialyzer Maxi, Novagen, UK). After dialysis, Alexa Fluor-488 fluorescence activity of the solution was confirmed by fluorimetry using a fluorescence spectrophotometer (Varian Cary Eclipse, USA). Uncoupled fluorophore or fluorophore aggregates, which might still be in solution after dialysis, did not accumulate at the gel surface or within the gel; fluorescence levels of unbound Alexa Fluor-488 within the gels and at the surface were comparable with those in solution, even at excessive concentrations (data not shown).

Gels were treated with varying concentrations of PDL tagged with Alexa Fluor-488 (PDL-Alexa), washed, and then examined with epifluorescence and confocal laser scanning microscopy (cLSM) (LSM 510, Zeiss, Germany; 25× water immersion objective, NA = 0.8; excitation source: HBO lamp and argon ion laser, respectively). In epifluorescence, images were recorded with a CCD camera (Pike, Allied Vision Technologies, Germany); in cLSM, z-stacks were recorded. Camera settings and scanning parameters were kept constant for the different gels. Median values of fluorescence intensities were determined with Corel Photo Paint X3 software for epifluorescence and with cLSM software (Zeiss LSM Image Browser) for confocal images.

The thickness of the gels was determined with cLSM in reflection mode. Measured z-distances between both substrate surfaces were corrected for the refractive index of the PAA gels ($n = 1.35$, measured with an Abbe refractometer, Bellingham and Stanley Ltd, UK) according to Snell's law.

2.5. Cell culture

All animal experiments were conducted in accordance with the United Kingdom Animals (Scientific Procedure) Act of 1986 and institutional guidelines. Pure astrocyte cultures were prepared from neonatal Sprague-Dawley rat cerebral cortices, as previously described [50] with some modifications. Briefly, neonates at P0–P2 were decapitated and the brain hemispheres were explanted and washed in Hanke's balanced salt solution (HBSS, Gibco, UK). Cortices were dissected, demembraned, minced into ∼1 mm^3 pieces, and incubated in 0.1% trypsin at 37 °C for 30 min. The mixture was then triturated using

triturating solution (300 mg BSA, 1 mg DNAase and 50 mg trypsin inhibitor in 100 ml HBSS) and the suspension was centrifuged for 5 min at 168 g and re-suspended in Dulbecco's modified Eagle's medium (DMEM; Gibco, UK) + 10% fetal calf serum (FCS; Gibco) + 1% penicillin–streptomycin, which will be referred to as 'culture medium' in the remainder of this text. The cell suspension acquired from each fetal cortex was seeded into one 75 cm^3 flask coated with PDL. The culture medium was changed the next day and afterward twice a week. After the cultures became confluent (7–10 days), they were agitated in a shaker-incubator overnight at 132 rpm with 2 cm radial amplitude to dislodge inflammatory cells and oligodendrocytes, resulting in pure astrocyte cultures. The medium was renewed the next day, and pure astrocytes were then used for the experiments.

After PAA gels were treated with PDL and washed, they were immersed in culture medium for 1 h before cell seeding. Pure astrocyte cultures were washed with DMEM and treated with ready-to-use trypsin-EDTA (Gibco) for 10 min at 37 °C in a CO_2 incubator. After adding culture medium and pipetting the cells, the cell suspension was centrifuged at 212 g for 5 min and the cells were then re-suspended in culture medium. PAA gels were placed in a culture dish covered with sterile parafilm. 5×10^5 astrocytes suspended in 300 μl culture medium were added onto each gel. The gels were returned to an incubator (37 °C, 5% CO_2), and after 1 h, they were gently placed in another 35 mm culture dish filled with 3 ml pre-incubated culture medium.

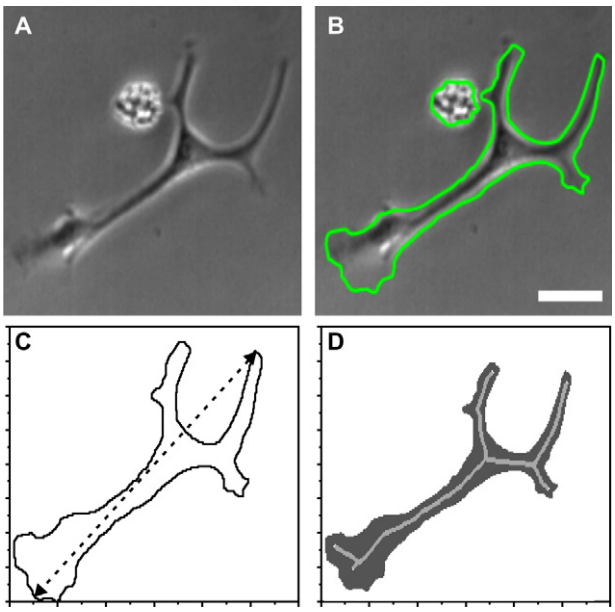

Figure 1. Illustration of automated cell morphometry. To analyze cell morphology, phase contrast images were taken (A), the cell contours were manually drawn (B), and subsequently automatically detected. A sample cell is represented in terms of its perimeter (closed line in (C)), diameter (dotted arrow in (C)), area (shadowed field in (D)), and its respective skeleton (bright lines (D)). The number of extremities obtained for this particular example is equal to five. Scale bar: 40 μm.

2.6. Quantitative morphometry

Phase contrast images of all cells along an arbitrary diameter of each PAA gel (46–474 cells/gel in 5–8 fields of view) were taken using an inverted microscope (Motic AE31, UK) equipped with a CCD camera (moticam 2000) and accompanying software (Motic Images Plus 2.0).

The quantification of the cells' morphological properties required two main steps: (i) extraction of each cell in the images from the respective background, a process called *segmentation* [51]; and (ii) calculation of several features describing complementary aspects of the geometrical properties of the cells. Because of the varying contrast and superposition/juxtaposition of cells, and in order to ensure proper selection of valid cells against residual traces, the segmentation of the cells was performed manually by delineating their contour using Corel Draw X3 software. Each cell was subsequently processed in a fully-automated fashion in order to derive a broad set of morphological features including: perimeter (P), area (A), diameter (D), elongation (E), number of extremities (N) and overall complexity (C). Each cell was mapped into a vector, $\vec{f}$, containing a comprehensive description of its morphological properties. The perimeter of each cell corresponds to the arc-length of its border, and was determined by tracking the cell contour using a chain-code algorithm [51]. The area was calculated by counting the number of pixels inside its detected contour. The diameter is defined as the largest distance between any pair of pixels of the cell [51]. The elongation was obtained through a spectral approach, which involved the determination of the eigenvalues of the covariance matrix defined by the coordinates of the cell pixels. More specifically, the elongation of a cell is defined as the ratio between the largest and smallest eigenvalues, which correspond to the variances of the cell coordinates along its major and minor axes of inertia [51]. As such, this morphological measurement is related to the elongation of an ellipse fitted to the original cell. This approach is particularly robust to noise in the cell shape. The number of extremities, a meaningful way to express the development of a cell, was obtained through the determination of the cells' skeleton and then counting the number of skeleton extremities. As illustrated in figure 1, the skeleton of a cell corresponds to a tree whose segments follow the middle parts of each elongated portion of the cell. Skeletons were obtained using the methodology described in da F Costa, 2003 [52], which involved the propagation of labels associated to the arc-length value along the cell contour. The cells' complexity was also quantified from their respective skeleton, being defined as the number of pixels in the skeleton divided by the diameter of the cell. The higher the complexity, the more curved and intricate the shape of the cell. For instance, a simple elongated cell would have a number of pixels of its skeleton similar to its diameter, leading to a complexity value close to one.

In order to obtain a more objective identification of the developmental stage of each cell, we applied an artificial intelligence methodology based on supervised classification. A set of 20 representative cells of each of the five defined spreading and adhesion categories were selected as prototypes, their morphological features were estimated as explained

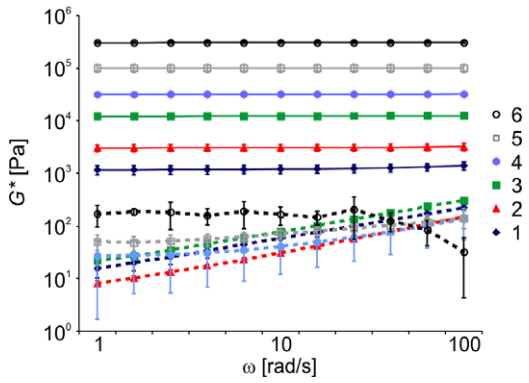

Figure 2. Rheological bulk measurements of PAA gels. Shown are the frequency-dependent storage moduli, G' (solid lines), and loss moduli, G'' (dotted lines), for the six different PAA gels described in table 1 (mean ± S.E.M., $N = 3$ for each gel type). The labels of the different symbols correspond to the numbers in table 1.

above and then used to train the supervised pattern recognition system. The automated identification of the cell category was performed by the k-neighbors approach [51, 53], which involves comparing the morphological properties of each cell with the properties of all prototypes. It can be shown that this approach converges to optimal classification performance (with respect to reducing the overall number of misclassifications) when the number of prototypes is relatively large [53].

2.7. Statistical analysis

Mann-Whitney tests were applied to assess the significance of differences between experimental groups.

3. Results and Discussion

3.1. Optimization of the PAA substrates

3.1.1. Bulk rheology of PAA substrates. Combinations of AA and Bis-A concentrations were chosen to establish six gels of different stiffness (table 1). The bulk mechanical properties were measured using a rheometer. The gels' elastic (storage) moduli G' and viscous (loss) moduli G'' are shown in figure 2. As frequency increased, the dominating G' remained approximately constant while G'' varied, which shows that the gels were stably crosslinked [17]. Creep measurements confirmed the almost purely elastic behavior of the gels (data not shown).

A word of caution might be appropriate at this point. There are several combinations of AA and Bis-A that can lead to the same storage modulus. For example, 7.5% AA and 0.02% Bis-A resulted in an identical storage modulus to 5% AA and 0.07% Bis-A. However, not all of these combinations are useful for the intended purpose of creating featureless homogeneous surfaces. The unidirectional expansion of gels attached to a surface during swelling in solvent results in local buckling of the free surfaces and the formation of creases in soft gels with an unfavorable AA:Bis-A ratio due to a mechanical instability [54]. This phenomenon is visible in figures 3(A) and (B), where a combination of 7.5% AA and 0.02% Bis-AA was used. Cells tended to migrate towards and align along creases, which run along the surface (figure 3(C)). The fact that cells align along these creases is likely an example of cell guidance by topological heterogeneities, which are interesting in their own right, but which need to be avoided in the context of the present study. The creases could be circumvented by choosing a different combination of AA and Bis-A with more crosslinker and less polymer but the same elastic modulus.

A minor additional, practical problem is the opaqueness of PAA gels with Bis-A concentrations above 0.5%, which appear milky and prevent acquisition of useful images. The six combinations of AA and Bis-A used in our experiments (table 1) represent the ultimate convergence of a long series of tests with the goal of optimizing all relevant features.

3.1.2. Microscopic homogeneity of PAA substrates tested with SFM. Bulk rheology averages compliance over the entire sample and might, thus, obscure local variations in the mechanical properties of the substrate surface. Since cells are able to discern and react to gradients in mechanical stiffness on the micron-scale [11, 55–57], it was important to test the mechanical homogeneity of the substrates. Force–indentation

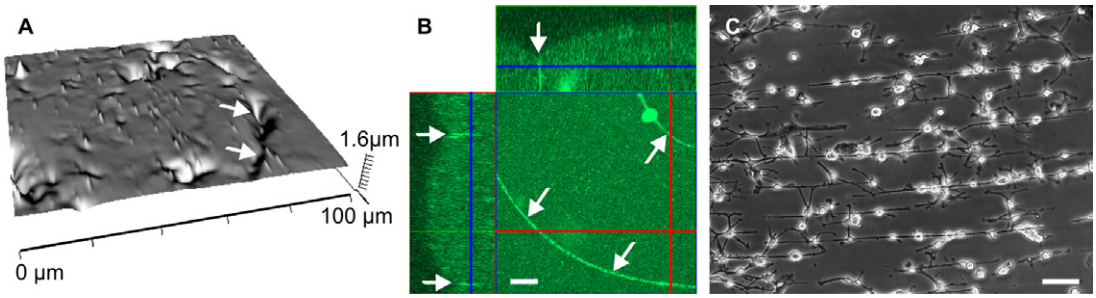

Figure 3. Effect of surface topological cues on astrocyte growth. PAA gels produced with an unfavorable AA:Bis-A ratio may buckle locally and form creases [54]. (A) An SFM surface scan of a PAA gel made from a combination of 7.5% AA and 0.02% Bis-AA shows such creases (arrows). (B) Reconstructed confocal z-stack of a fluorescently labeled PAA gel of the same composition in cross-section; arrows indicate surface features. The lines in the top view indicate the locations for the cross-sections visible at its left and top sides. The lines in the cross-sections show the level of the top view. (C) If astrocytes are cultured on substrates with creases, which in this example are running horizontally, they often extend processes along those topological cues. Scale bars: 50 μm in (B), 60 μm in (C).

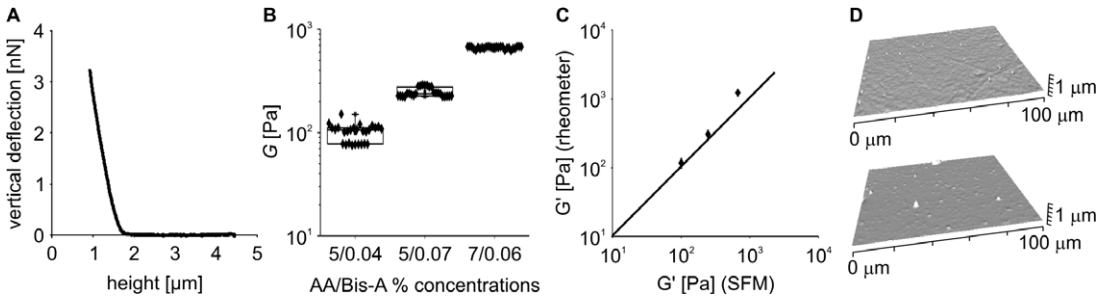

Figure 4. Local homogeneity of PAA substrates measured by SFM. (A) A typical force–indentation curve obtained on PAA gels using SFM. (B) Box plots and data points of local shear moduli G obtained from SFM measurements. Shown are data from three different AA/Bis-A combinations, which result in bulk shear storage moduli G' of ∼100, 300 and 1000 Pa (cf table 1). The SFM measurements were in good agreement with the bulk rheology data. For each AA/Bis-A combination, three gels were measured at nine points each. Note that the gels were very homogeneous. (C) Direct comparison of the shear moduli obtained with bulk rheometry and SFM on three identical gels. The solid line indicates the line of ideal agreement. (D) Surface topography of compliant ($G' = 100$ Pa; top), and stiff ($G' = 10$ kPa; bottom) substrates imaged with SFM. Note that the PAA gel surfaces are very smooth.

curves (figure 4(A)) were acquired with SFM on PAA gels and analyzed by custom-built software. The extracted Young's modulus values E were converted into the shear modulus G by the relation $G = \frac{E}{2(1+\nu)}$ (assuming a Poisson's ratio of $\nu = 0.48$ [49]), and the results are shown in figure 4(B). The values were homogeneous across the surface of each of the substrates. Since the shear storage modulus $G'(\omega)$ determined with bulk rheology was largely independent of the angular frequency, a comparison with the static shear modulus G measured with SFM was possible, and revealed that the values were in good agreement (figure 4(C)).

A further concern regarding the microscopic surface homogeneity relates to the topological features present, because cells can also react to those as guidance cues [28]. The results of SFM scans in the contact mode of substrates at two extremes of compliance are shown in figure 4(D). Within an area of 100 μm × 100 μm, the average roughness $R_a = \frac{1}{n}\sum_{i=1}^{n}|y_i|$ of PAA gels with $G' = 100$ Pa was 9.8 nm ± 1.4 nm ($N = 8$, mean ± S.E.M.), that of gels with $G' = 10$ kPa was 4.3 nm ± 0.3 nm ($N = 5$). Larger features visible in the images are likely due to dirt acquired over the duration of the scanning or artifacts due to transient sticking of the scanning probe to the surface (figure 4(D)); neither should be relevant when culturing cells. Overall, the surfaces were demonstrably homogeneous in both their microscopic mechanical properties and surface topology, thus ensuring no unintended cues apart from bulk mechanics.

3.1.3. PDL coating amount and homogeneity assessed by fluorescence microscopy. The last remaining aspect related to unwanted cell signaling cues is the coating of the surface with an adhesion-promoting substance, as discussed in the introduction. PAA gels by themselves are inert and do not favor cell adhesion, so that coating with a cytophilic agent is necessary. In this study, we used PDL, which primarily facilitates cell adhesion by unspecific Coulomb attraction between its positive charge and the cells' overall negative charge. However, PDL may adsorb serum or cell-secreted proteins such as fibronectin and thereby produce specific but unknown ligations—a problem inherent to all cell culture surfaces. This problem can be minimized by ensuring the same coating density of PDL and thus adsorbed proteins: in this case, the effect of specific ligations will be the same on all substrates, and differences between cell populations will only be due to the differences in mechanical substrate properties. Interestingly, we did not observe any major differences in morphology of cells cultured on PDL-coated and laminin-coated surfaces (data not shown).

Several approaches have been used to functionalize the surface of PAA gels. Three of the most frequently used methods include the application of a nonaqueous layer of toluene containing 0.5% acrylic acid *N*-hydroxy succinimide (NHS) ester during polymerization [23, 42], UV treatment of Sulfo-SANPAH after polymerization [10, 14, 15, 19, 24, 34, 39], and the application of hydrazine hydrate [44]. In our experiments, we have chosen hydrazine hydrate treatment of the gels, because it resulted in the strongest and most homogeneous surface coating. However, it needs to be stated that hydrazine hydrate changes the pH of the PAA gels towards the basic region, and the subsequent treatment of the gels with acetic acid needs to be well timed to achieve gels with a neutral pH.

Since cells are known to respond to surface patterning of adhesion molecules [24, 58], it is important to test the homogeneity of the coating. The use of fluorescently labeled PDL allowed us to spatially resolve the coating distribution at the gel surface, in contrast to spatially insensitive methods such as radioactive labeling [38]. The resolution of fluorescence microscopy, however, is in the hundreds of nm range; coating heterogeneities below that range cannot be resolved. PAA gels treated with PDL-Alexa solution were imaged with both epifluorescence, as described in previous reports [14, 19, 23, 42], and confocal laser scanning microscopy (cLSM). Figure 5 shows the resulting images obtained with the respective methods on 100 Pa and 10 kPa gels treated with 10 μg ml^{-1} PDL-Alexa.

Epifluorescence images showed rather homogeneous and continuous coating in both instances, which confirms previous reports in the literature [14, 42]. However, cLSM images revealed a homogeneous but spotty fluorescence pattern, which

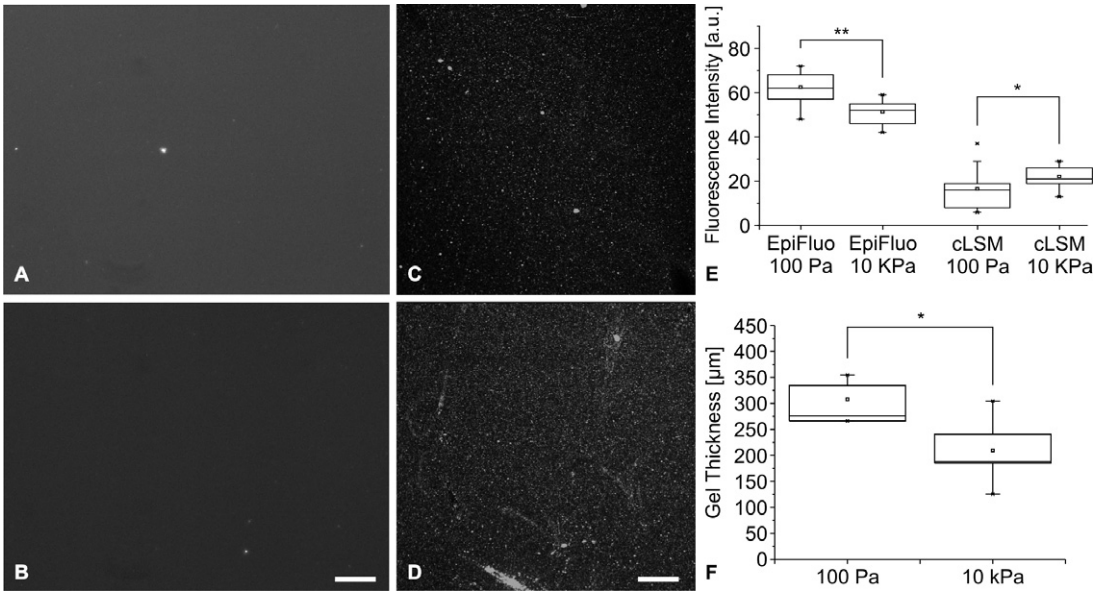

Figure 5. Fluorescence microscopy of PDL-Alexa coating. Epifluorescence images of (A) 100 Pa and (B) 10 kPa PAA gels and cLSM images of (C) 100 Pa and (D) 10 kPa PAA gels, all treated with 10 μg ml^{-1} PDL-Alexa. While in epifluorescence the signal is rather homogeneous, in cLSM bright dots dominate the fluorescence signal. (E) Quantitative comparison of the fluorescence signal of the two different gel types obtained by the two different fluorescence techniques ($N = 3$ in each experiment). (F) Shows the thickness of the gels whose fluorescence signal intensity is plotted in (E). * $P < 0.05$; ** $P < 0.01$ (Mann-Whitney Test); scale bars are 20 μm in (A) and (B), and 50 μm in (C) and (D).

has to our knowledge not been described before (figures 5(C) and (D)). This difference probably results from the different imaging volumes being sampled by the two techniques. In epifluorescence, the fluorescence emitted from the entire illuminated cone of excitation light contributes to the signal imaged. Since PDL-Alexa can easily penetrate the PAA meshwork, epifluorescence is sensitive to the absolute uptake of PDL into the extended bulk of the gel, rather than merely the surface coating. Confocal microscopy, on the other hand, rejects out-of-focus light and more faithfully reports the coating actually present at the surface. It is, thus, not surprising, that certain features of the PDL-Alexa coating at the surface, such as the spottiness, are visible in cLSM but are smeared out and obscured in epifluorescence. Apparently, PDL-Alexa accumulates in tiny clusters at the surface of the PAA gels in addition to a smooth background coating. The mechanism of this clustering is beyond the scope of this article; its impact on biological function will be addressed below.

In addition, a quantitative analysis of the average fluorescence signal revealed contrary trends between compliant and stiff gels (figure 5(E)). While in epifluorescence the soft gels showed more signal, and thus PDL uptake, than the stiff ones, the situation was reversed in the cLSM measurements. This can probably be explained by the greater swelling of the more compliant gels: although the volume of soft and stiff gels was initially the same (i.e., 60 μl), the height of the more compliant gels increased by 50% (figure 5(F)). This also increased their final volume and contributed more total signal in epifluorescence. In cLSM, only a thin layer of fixed thickness at the surface is imaged, which is less dense in the more compliant and swollen gel, so that the fluorescence in this layer is stronger in the stiffer gel. The influence of this slight difference in surface coating on the cells' behavior is addressed below. The difference in the absolute amount of fluorescence detected by the two techniques is irrelevant since neither the CCD camera in epifluorescence nor the photo-multiplier tube in cLSM were calibrated to a common standard. Both imaging methods, however, demonstrate that the large-scale PDL-distribution is homogeneous, so that this last parameter is under control and substrate mechanics can be controlled independently of mechanical, topographical or surface chemical heterogeneities, which could otherwise adversely skew results.

3.2. Astrocyte response to PAA substrates

3.2.1. Astrocyte cultures on substrates of different compliance. Primary pure rat astrocyte cultures were seeded onto PAA substrates of six different compliances (according to table 1). Phase contrast images were recorded after 1 day, when most cells were still spatially separated from each other. Typical cell examples for the most compliant substrate ($G' = 100$ Pa) and for one two orders of magnitude stiffer ($G' = 10$ kPa) are shown in figure 6. Astrocytes cultured on compliant substrates had a different phenotype than those cultured on stiff substrates, as has been previously described [39, 42, 43]. The first were generally rounded up (but firmly attached), while the latter displayed on average a much more spread morphology with some cells having several distinct processes. From visual inspection of the images it was very obvious that intermediate compliances showed similar results, with a relatively sharp transition from compliant to stiff phenotype at around $G' = 1$ kPa.

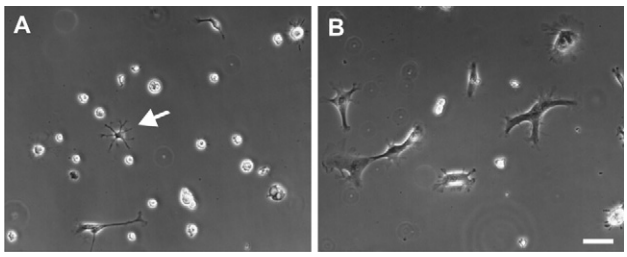

Figure 6. Phase contrast images of astrocytes cultured on differently compliant substrates. Astrocytes on PAA gels with storage moduli of (A) $G' = 100$ Pa are often rounded up even after being in culture for days. Astrocytes extending processes frequently assume a star-like shape (arrow). (B) Astrocytes cultured on gels with $G' = 10$ kPa spread well and resemble those grown on tissue culture plastics. Scale bar: 60 μm.

3.2.2. Quantitative morphometric analysis of astrocyte growth. While the difference in cell growth and spreading on compliant and stiff substrates is qualitatively obvious by eye, it is desirable to capture these differences in an automated, quantitative fashion using rigorously defined morphological features. In this study we made use of the tools established in neuroscience, where they have been developed to characterize the intricate shapes of the many different types of neurons [51]. Astrocytes were cultured on compliant ($G' = 100$ Pa) and stiff ($G' = 10$ kPa) substrates coated with 0, 1, 10, 100, or 1000 μg ml^{-1} PDL. The cell contours were outlined by hand and then automatically analyzed for perimeter (P), area (A), diameter (D), elongation (E), number of extremities (N) and overall complexity (C), as defined in section 2. Our results are summarized in figure 7 and table 2. All investigated cell morphological parameters (P, A, D, E, N, and C) were significantly smaller in the compliant phenotype if compared to the stiff phenotype. The dependence of the cells' morphology on PDL coating density seemed to be weak, if compared to the effect of the substrate stiffness, and slightly biphasic, with a maximum at 10–100 μg ml^{-1} PDL concentration. These data correspond well to those previously published on the dependence of aortic smooth muscle cell area on substrate stiffness and collagen coating density [10]. Also, in that study, the substrate stiffness did override the effect of the collagen density, and the cell area showed a biphasic change with increasing collagen concentration.

Table 2. Number of astrocytes analyzed and shown in figures 7 and 8 (mean ± S.E.M.) taken from 3 different cultures.

PDL concentrations (μg ml^{-1})	100 Pa PAA gel	10 kPA PAA gel
0	69.5 ± 33.23	159.5 ± 137.89
1	420 ± 65.05	290 ± 49.50
10	415 ± 83.44	311 ± 5.66
100	323.5 ± 30.41	313 ± 24.04
1000	122 ± 57.98	157.5 ± 26.16

In addition to these various independent descriptors of cell morphology, we also used an artificial intelligence-based, supervised pattern recognition algorithm to identify linear combinations that best described five different morphological states identified by an expert. These states were assigned morphological scores from 1–5, with 1 being round and 5 being fully spread and differentiated (figure 8(A)). This algorithm, which considered all quantitative parameters described above, was then used to automatically classify all cells in the various experimental conditions. The average morphological score of cells grown on stiffer substrates at all coating densities was significantly higher than that of cells cultured on softer substrates (figures 8(B) and (C)). The scores determined

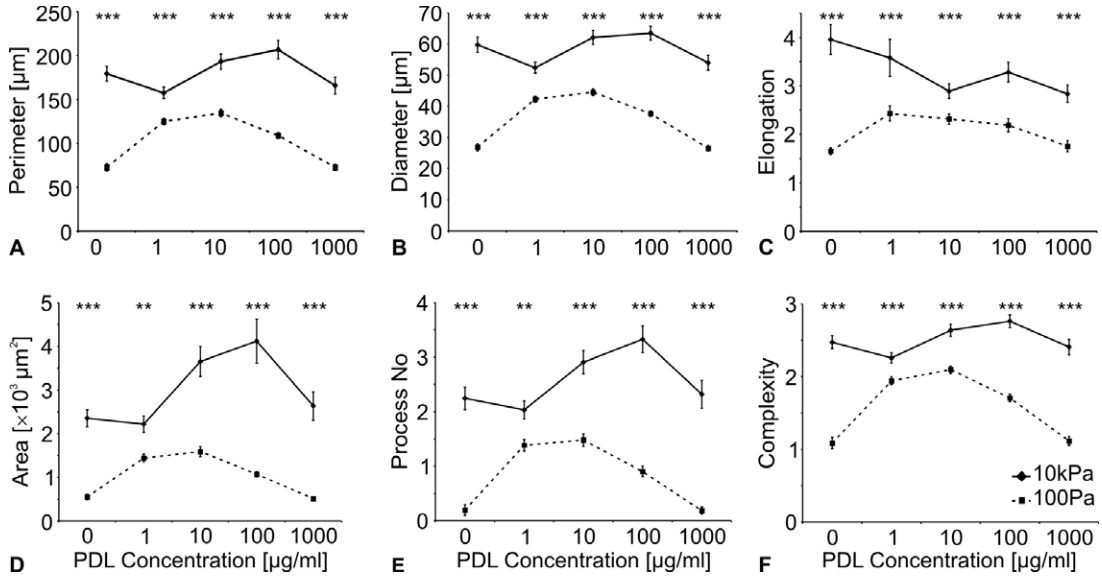

Figure 7. Quantitative morphological analysis of astrocytes. Astrocytes grown on PAA gels with $G' = 100$ Pa (dotted lines) and $G' = 10$ kPa (continuous lines) coated with increasing concentrations of PDL were analyzed for cell morphology parameters (cf section 2). At all PDL coating densities, perimeter (A), diameter (B), elongation (C), area (D), the number of processes (E), and the cells' complexity (F) were significantly larger if astrocytes were cultured on stiffer gels (** $P < 0.01$; *** $P < 0.001$; Mann-Whitney Test). The compliance of the gels seemed to be more important for the development of the investigated cell morphological features than the level of PDL coating.

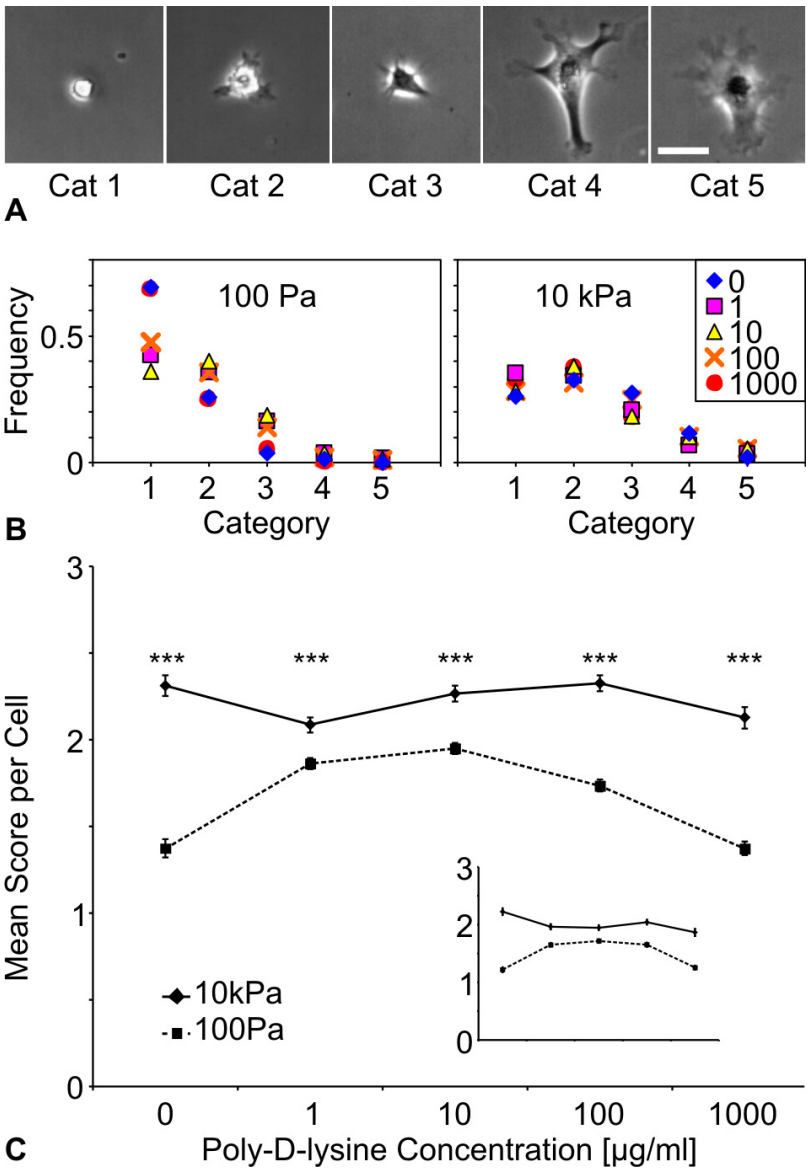

Figure 8. Artificial intelligence-based analysis of astrocyte morphology. (A) Astrocytes were divided into five categories according to their different shapes. (B), (C) Cells cultured on PAA gels with $G' = 100$ Pa (dotted line) and 10 kPa (continuous line) were analyzed with an artificial intelligence-based shape analysis, which was previously trained with samples of the morphological categories shown in (A), considering all parameters shown in figure 7. (B) Relative distribution of cell scores on compliant (left) and stiff (right) substrates. The symbols represent different amounts of PDL coating as indicated in the inset. (C) Average scores are plotted in dependence of the PDL concentration. Astrocytes cultured on stiff gels showed significantly more spread and advanced morphology than those cultured on compliant gels, which is consistent with the manual control classification of the same cells (inset in (C)). Scale bar: 40 μm; *** $P < 0.001$ (Mann-Whitney Test).

automatically were in excellent agreement with the manual control classification of the same cells (inset in figure 8(C)).

Again, there seemed to be a dependence of the results on coating density, with maximum scores at 10–100 μg ml^{-1} PDL concentration. Since we used PDL, which provides a fairly unspecific binding of cells to the surface by electrostatic interaction, and it is known that, once adhered, these cells start to secrete their own specific ECM proteins for further engagement with the surface [59], it is to be expected that the cells should to some extent react to the amount of PDL laid down on the surface. First, increasing amounts of PDL should lead to increasing cell attachment and spreading, but once the cell is sufficiently spread and starts to supply its own ECM, any further increase in PDL might adversely compete with the native ECM put down and lead to a (slight) decrease in cell spreading. Alternatively, the strong surface adhesion and the tension thus induced in the cell membrane [60] might decrease cell activity. There might also be a temporal component to this, with cells on surfaces with little PDL probably requiring more time to adhere and to secrete more ECM, an aspect which is not captured in the present study as all cells were evaluated after the same time. Overall, however, our analysis quantitatively shows that the effect of the amount of coating on cell morphology is rather small if compared to the effect of the mechanical properties of the cell substrate.

4. Summary and conclusion

In this study, we investigated the growth and spreading response of primary astrocytes as a function of substrate compliance and PDL coating density, in order to shed light on the innate mechanosensitivity of these cells. We optimized the commonly used PAA gels to avoid mechanical, topological, and polypeptide coating inhomogeneities, which otherwise could provide unwanted cues (figures 2–5). Our quantitative morphological analysis revealed that astrocytes spread more and have a more complex shape on stiffer substrates, which resembles their morphology if grown on tissue culture plastics or glass (figures 6–8). These results are in line with previous, more qualitative reports [39, 42, 43] and differ from the behavior of neurons, which seem to prefer more compliant substrates with storage moduli G' of a few hundred Pa [34, 42]. It should be noted, however, that astrocytes grown on soft substrates more closely resemble the star-like shape of astrocytes *in vivo* (figure 6(A)).

Astrocyte activation *in vivo*, as found in numerous pathological alterations of the nervous system, is characterized by increased expression of intermediate filaments, cell spreading, growth, and proliferation [61]. If the stiffness of the cellular environment contributes to astrocyte activation, then the activation threshold should be expected at the upper end of the stiffness range found in the CNS. This upper end is about $G' \approx 1$ kPa ([62] and unpublished data), which is in agreement with our experiments determining the relatively sharp transition from the compliant to stiff astrocyte phenotype. Intriguingly, astrocytes make up the largest fraction of cells recruited to glial scars, which inevitably form after trauma to the CNS. Given that glial scars are stiffer than regular CNS tissue, which is widely suspected, it is not unlikely that at least some of the accumulation of astrocytes in these scars could be due to their mechanosensitive response investigated in this study. Our results could thus lead to a better understanding of CNS physiology and pathology, and they could open novel avenues for treating associated disorders.

Acknowledgments

The authors would like to thank Christine Holt, Paul Janmey, Drew Murray, Alex Winkel, Fardad Taghizadeh-Afshari, Ruma Raha-Chowdhury, Jessica Kwok, David Story, Kevin Chalut, Eugene Terentjev, and Ulrich Steiner for inspiring discussions and technical help. Furthermore, we thank Erika Eiser for access to the rheometer and Aubrey Lambert (Zeiss, UK) for loan of the water dipping objective. We acknowledge financial support from Cambridge Overseas Trust (ORS equivalent bursary) to PM, from FAPESP (05/00587-5) and CNPq (301303/06-1) to LdFC, from EPSRC and JPK for a CASE studentship (KNZA/083) to AC, from the Royal Society for a University Research Fellowship to SPL, from EPSRC RCUK—Basic Technology Program Contract EP/C52330X/1 to JF/SPL/JG, and from the Alexander von Humboldt Foundation (Feodor Lynen Fellowship) to KF.

References

[1] Zajac A L and Discher D E 2008 Cell differentiation through tissue elasticity-coupled, myosin-driven remodeling *Curr. Opin. Cell Biol.* **20** 609–15
[2] Janmey P A and McCulloch C A 2007 Cell mechanics: integrating cell responses to mechanical stimuli *Annu. Rev. Biomed. Eng.* **9** 1–34
[3] Discher D E, Janmey P and Wang Y L 2005 Tissue cells feel and respond to the stiffness of their substrate *Science* **310** 1139–43
[4] Franze K *et al* 2009 Neurite branch retraction is caused by a threshold-dependent mechanical impact *Biophys. J.* **97** 1883–90
[5] Rehfeldt F, Engler A J, Eckhardt A, Ahmed F and Discher D E 2007 Cell responses to the mechanochemical microenvironment–implications for regenerative medicine and drug delivery *Adv. Drug Deliv. Rev.* **59** 1329–39
[6] Bischofs I B and Schwarz U S 2003 Cell organization in soft media due to active mechanosensing *Proc. Natl Acad. Sci. USA* **100** 9274–9
[7] Bershadsky A, Kozlov M and Geiger B 2006 Adhesion-mediated mechanosensitivity: a time to experiment, and a time to theorize *Curr. Opin. Cell Biol.* **18** 472–81
[8] Yeung T *et al* 2005 Effects of substrate stiffness on cell morphology, cytoskeletal structure, and adhesion *Cell Motil. Cytoskeleton.* **60** 24–34
[9] Irwin E F, Saha K, Rosenbluth M, Gamble L J, Castner D G and Healy K E 2008 Modulus-dependent macrophage adhesion and behavior *J. Biomater. Sci. Polym. Edn* **19** 1363–82
[10] Engler A, Bacakova L, Newman C, Hategan A, Griffin M and Discher D 2004 Substrate compliance versus ligand density in cell on gel responses *Biophys. J.* **86** 617–28
[11] Byfield F J 2009 Absence of filamin A prevents cells from responding to stiffness gradients on gels coated with collagen but not fibronectin *Biophys. J.* **96** 5095–102
[12] Ulrich T A, Pardo E M D and Kumar S 2009 The mechanical rigidity of the extracellular matrix regulates the structure, motility, and proliferation of glioma cells *Cancer Res.* **69** 4167–74
[13] Hsiong S X, Carampin P, Kong H J, Lee K Y and Mooney D J 2008 Differentiation stage alters matrix control of stem cells *J. Biomed. Mater. Res.* A. **85** 145–56
[14] Rowlands A S, George P A and Cooper-White J J 2008 Directing osteogenic and myogenic differentiation of MSCs: interplay of stiffness and adhesive ligand presentation *Am. J. Physiol. Cell Physiol.* **295** C1037–44
[15] Pelham R J Jr and Wang Y 1997 Cell locomotion and focal adhesions are regulated by substrate flexibility *Proc. Natl Acad. Sci. USA* **94** 13661–5
[16] Lo C M, Wang H B, Dembo M and Wang Y L 2000 Cell movement is guided by the rigidity of the substrate *Biophys. J.* **79** 144–52
[17] Hynes S R, Rauch M F, Bertram J P and Lavik E B 2009 A library of tunable poly(ethylene glycol)/poly(L-lysine) hydrogels to investigate the material cues that influence neural stem cell differentiation *J. Biomed. Mater. Res.* A **89** 499–509
[18] Frey M T and Wang Y L 2009 A photo-modulatable material for probing cellular responses to substrate rigidity *Soft Matter* **5** 1918–24
[19] Stroka K M and Aranda-Espinoza H 2009 Neutrophils display biphasic relationship between migration and substrate stiffness *Cell Motil. Cytoskeleton* **66** 328–41
[20] Engler A J, Sen S, Sweeney H L and Discher D E 2006 Matrix elasticity directs stem cell lineage specification *Cell* **126** 677–89
[21] Guilak F, Cohen D M, Estes B T, Gimble J M, Liedtke W and Chen C S 2009 Control of stem cell fate by physical

interactions with the extracellular matrix *Cell Stem Cell* **5** 17–26
[22] Discher D E, Mooney D J and Zandstra P W 2009 Growth factors, matrices, and forces combine and control stem cells *Science* **324** 1673–7
[23] Winer J P, Janmey P A, McCormick M E and Funaki M 2009 Bone marrow-derived human mesenchymal stem cells become quiescent on soft substrates but remain responsive to chemical or mechanical stimuli *Tissue Eng.* A **15** 147–54
[24] Engler A J, Griffin M A, Sen S, Bonnemann C G, Sweeney H L and Discher D E 2004 Myotubes differentiate optimally on substrates with tissue-like stiffness: pathological implications for soft or stiff microenvironments *J. Cell Biol.* **166** 877–87
[25] Levy-Mishali M, Zoldan J and Levenberg S 2009 Effect of scaffold stiffness on myoblast differentiation *Tissue Eng.* A **15** 935–44
[26] Ingber D E 2003 Mechanobiology and diseases of mechanotransduction *Ann. Med.* **35** 564–77
[27] Jaalouk D E and Lammerding J 2009 Mechanotransduction gone awry *Nat. Rev.* **10** 63–73
[28] Mitragotri S and Lahann J 2009 Physical approaches to biomaterial design *Nat. Mater.* **8** 15–23
[29] Plant A L, Bhadriraju K, Spurlin T A and Elliott J T 2009 Cell response to matrix mechanics: focus on collagen *Biochim. Biophys. Acta* **1793** 893–902
[30] Reed J, Walczak W J, Petzold O N and Gimzewski J K 2009 *In situ* mechanical interferometry of matrigel films *Langmuir* **25** 36–9
[31] Ju Y E, Janmey P A, McCormick M E, Sawyer E S and Flanagan L A 2007 Enhanced neurite growth from mammalian neurons in three-dimensional salmon fibrin gels *Biomaterials* **28** 2097–108
[32] Georges P C and Janmey P A 2005 Cell type-specific response to growth on soft materials *J. Appl. Physiol.* **98** 1547–53
[33] Benya P D and Shaffer J D 1982 Dedifferentiated chondrocytes reexpress the differentiated collagen phenotype when cultured in agarose gels *Cell* **30** 215–24
[34] Flanagan L A, Ju Y E, Marg B, Osterfield M and Janmey P A 2002 Neurite branching on deformable substrates *Neuroreport* **13** 2411–5
[35] Yu X J and Bellamkonda R V 2001 Dorsal root ganglia neurite extension is inhibited by mechanical and chondroitin sulfate-rich interfaces *J. Neurosci. Res.* **66** 303–10
[36] Jeon O, Bouhadir K H, Mansour J M and Alsberg E 2009 Photocrosslinked alginate hydrogels with tunable biodegradation rates and mechanical properties *Biomaterials* **30** 2724–34
[37] Willits R K and Skornia S L 2004 Effect of collagen gel stiffness on neurite extension *J. Biomater. Sci.* **15** 1521–31
[38] Leach J B, Brown X Q, Jacot J G, Dimilla P A and Wong J Y 2007 Neurite outgrowth and branching of PC12 cells on very soft substrates sharply decreases below a threshold of substrate rigidity *J. Neural Eng.* **4** 26–34
[39] Jiang X *et al* 2007 Cell growth in response to mechanical stiffness is affected by neuron-astroglia interactions *Open Neurosci. J.* **1** 7–14
[40] Munevar S, Wang Y and Dembo M 2001 Traction force microscopy of migrating normal and H-ras transformed 3T3 fibroblasts *Biophys. J.* **80** 1744–57
[41] Janmey P A, Winer J P, Murray M E and Wen Q 2009 The hard life of soft cells *Cell Motil. Cytoskeleton* **66** 597–605
[42] Georges P C, Miller W J, Meaney D F, Sawyer E S and Janmey P A 2006 Matrices with compliance comparable to that of brain tissue select neuronal over glial growth in mixed cortical cultures *Biophys. J.* **90** 3012–8
[43] Jiang F X, Yurke B, Firestein B L and Langrana N A 2008 Neurite outgrowth on a DNA crosslinked hydrogel with tunable stiffnesses *Ann. Biomed. Eng.* **36** 1565–79
[44] Damljanovic V, Lagerholm B C and Jacobson K 2005 Bulk and micropatterned conjugation of extracellular matrix proteins to characterized polyacrylamide substrates for cell mechanotransduction assays *Biotechniques* **39** 847–51
[45] Mahaffy R E, Park S, Gerde E, Kas J and Shih C K 2004 Quantitative analysis of the viscoelastic properties of thin regions of fibroblasts using atomic force microscopy *Biophys. J.* **86** 1777–93
[46] Mahaffy R E, Shih C K, MacKintosh F C and Kas J 2000 Scanning probe-based frequency-dependent microrheology of polymer gels and biological cells *Phys. Rev. Lett.* **85** 880–3
[47] Hutter J L and Bechhoefer J 1993 Calibration of atomic-force microscope tips *Rev. Sci. Instrum.* **64** 1868–73
[48] Hertz H 1881 Über die Berührung fester elastischer Körper *J. Reine Angew. Math.* **92** 156–71
[49] Boudou T, Ohayon J, Picart C and Tracqui P 2006 An extended relationship for the characterization of Young's modulus and Poisson's ratio of tunable polyacrylamide gels *Biorheology* **43** 721–8
[50] Wilby M J, Muir E M, Fok-Seang J, Gour B J, Blaschuk O W and Fawcett J W 1999 N-Cadherin inhibits Schwann cell migration on astrocytes *Mol. Cell. Neurosci.* **14** 66–84
[51] da F Costa L and Cesar R M Jr 2009 *Shape Analysis and Classification: Theory and Practice* 2nd edn (Boca Raton, FL: CRC Press)
[52] da F Costa L 2003 Enhanced multiscale skeletons *Real-Time Imaging* **9** 315–9
[53] Duda R O, Hart P E and Stork D G 2001 *Pattern Classification* (New York: Wiley)
[54] Trujillo V, Kim J and Heyward R 2008 Creasing instability of surface-attached hydrogels *Soft Matter* **4** 564–9
[55] Lo C M, Wang H B, Dembo M and Wang Y L 2000 Cell movement is guided by the rigidity of the substrate *Biophys. J.* **79** 144–52
[56] Wong J Y, Velasco A, Rajagopalan P and Pham Q 2003 Directed movement of vascular smooth muscle cells on gradient-compliant hydrogels *Langmuir* **19** 1908–13
[57] Isenberg B C, Dimilla P A, Walker M, Kim S and Wong J Y 2009 Vascular smooth muscle cell durotaxis depends on substrate stiffness gradient strength *Biophys. J.* **97** 1313–22
[58] Clark P, Britland S and Connolly P 1993 Growth cone guidance and neuron morphology on micropatterned laminin surfaces *J. Cell Sci.* **105** 203–12
[59] Smith-Thomas L C *et al* 1994 An inhibitor of neurite outgrowth produced by astrocytes *J. Cell Sci.* **107** 1687–95
[60] Hategan A, Law R, Kahn S and Discher D E 2003 Adhesively-tensed cell membranes: lysis kinetics and atomic force microscopy probing *Biophys. J.* **85** 2746–59
[61] Milenkovic I *et al* 2005 Pattern of glial fibrillary acidic protein expression following kainate-induced cerebellar lesion in rats *Neurochem. Res.* **30** 207–13
[62] Lu Y B *et al* 2006 Viscoelastic properties of individual glial cells and neurons in the CNS *Proc. Natl Acad. Sci. USA.* **103** 17759–64